Downloaded from genome.cshlp.org on October 3, 2011 - Published by Cold Spring Harbor Laboratory Press

Delineation of key regulatory elements identifies points of vulnerability in the mitogen-activated signaling network

Noor Jailkhani, Srikanth Ravichandran, Shubhada R Hegde, et al.

Genome Res. published online August 24, 2011
Access the most recent version at doi:10.1101/gr.116145.110

Supplemental Material	**http://genome.cshlp.org/content/suppl/2011/08/24/gr.116145.110.DC1.html**
P<P	Published online August 24, 2011 in advance of the print journal.
Accepted Preprint	Peer-reviewed and accepted for publication but not copyedited or typeset; preprint is likely to differ from the final, published version.
Email alerting service	Receive free email alerts when new articles cite this article - sign up in the box at the top right corner of the article or **click here**

Advance online articles have been peer reviewed and accepted for publication but have not yet appeared in the paper journal (edited, typeset versions may be posted when available prior to final publication). Advance online articles are citable and establish publication priority; they are indexed by PubMed from initial publication. Citations to Advance online articles must include the digital object identifier (DOIs) and date of initial publication.

To subscribe to *Genome Research* go to:
http://genome.cshlp.org/subscriptions

Copyright © 2011, Cold Spring Harbor Laboratory Press

Downloaded from genome.cshlp.org on October 3, 2011 - Published by Cold Spring Harbor Laboratory Press

DELINEATION OF KEY REGULATORY ELEMENTS IDENTIFIES POINTS OF VULNERABILITY IN THE MITOGEN-ACTIVATED SIGNALING NETWORK

Noor Jailkhani[1], Srikanth Ravichandran[1], Shubhada R. Hegde[2], Zaved Siddiqui[1], Shekhar C. Mande[2], and Kanury V.S. Rao[1,3]

[1]International Centre for Genetic Engineering and Biotechnology
Aruna Asaf Ali Marg
New Delhi – 110067
INDIA

[2]Centre for DNA Fingerprinting and Diagnostics
Gruhakalpa, 5-4-399B
Nampally
Hyderabad – 500001
INDIA

[3]Correspondence: Kanury V.S. Rao
Tel: 91-11-26176680
FAX: 91-11-26715114
Email: kanury@icgeb.res.in

Running title: Defining vulnerable nodes in mitogenic signaling.
Key words: Systems Biology, Network modules, siRNA, Cell cycle, Synthetic lethality.

Downloaded from genome.cshlp.org on October 3, 2011 - Published by Cold Spring Harbor Laboratory Press

ABSTRACT.

Drug development efforts against cancer are often hampered by the complex properties of signaling networks. Here we combined the results of an RNAi screen targeting the cellular signaling machinery, with graph theoretical analysis to extract the core modules that process both mitogenic and oncogenic signals to drive cell cycle progression. These modules encapsulated mechanisms for coordinating seamless transition of cells through the individual cell cycle stages and, importantly, were functionally conserved across different cancer cell types. Further analysis also enabled extraction of the core signaling axes that progressively guide commitment of cells to the division cycle. Importantly, pharmacological targeting of the least redundant nodes in these axes yielded a synergistic disruption of the cell cycle in a tissue-type independent manner. Thus the core elements that regulate temporally distinct stages of the cell cycle provide attractive targets for the development of multi-module based chemotherapeutic strategies.

Publicly available Protein-Protein interaction databases used in this study have been mentioned and also have been cited at the appropriate places in the text. Novoseek disease relationship scores were obtained from http://www.novoseek.com/Welcome.action. Supplementary materials include six additional figures and eight tables.

Downloaded from genome.cshlp.org on October 3, 2011 - Published by Cold Spring Harbor Laboratory Press

INTRODUCTION.

Current approaches aimed at anti-cancer drug development primarily focus on identifying those signaling intermediates where mutations have led to constitutive activity in a given cancer. The aim then is to develop inhibitors against these targets (Evan and Vousden 2001; Vermeulen et al. 2003). The prevailing systems view, however, describes the signaling machinery as being organized into a complex network (Barabasi and Oltvai 2004; Zhu et al. 2007) that exhibits a non-linear response behavior (Alon 2007). This implies that the effects of inhibiting an intermediate need not necessarily be the inverse of that which is obtained upon its constitutive activation. In this context, at least one factor influencing the outcome would be the level of functional redundancy exhibited by this intermediate (Edelman and Gally 2001; Tononi et al. 1999). That is, although activation of mitogenic pathways may derive from an oncogenic mutation in a given signaling intermediate, inhibition of this intermediate may however have only a minimal effect if its functional role is compensated for through contributions from other intermediates.

The above possibility is especially relevant for cancer cells where mutations in more than one signaling molecule is often the norm (Vogelstein and Kinzler 2004). In other words the greater degree of plasticity associated with oncogenic pathway activation, relative to its suppression, also indicates that the ideal targets for pathway inhibition need not necessarily coincide with those that are involved in its activation. Such increments to our understanding of the complex properties of biological systems illuminate that drug development efforts will be significantly aided by a better resolution of the signaling circuitry that controls cell cycle, as well as a description of the least redundant nodes (i.e. functionally least replaceable nodes) that participate in this process.

Downloaded from genome.cshlp.org on October 3, 2011 - Published by Cold Spring Harbor Laboratory Press

Despite accumulation of information on mitogen-activated signaling cascades a clear picture on how they integrate to modulate the cell cycle program is, however, still lacking (Papin et al. 2005). Indeed the current challenge is to develop approaches that can distill the available information, and provide a coherent view of the core pathways involved (Del Sol et al. 2010; Papin et al. 2005). In the present study we combined the results of a siRNA screen targeting the signaling machinery with graph theoretical analysis to extract the core modules that processed mitogenic signal in the context of the individual phases of the cell cycle. We demonstrate that these modules indeed constitute functionally conserved features of mitogen dependent signaling networks, and that the least redundant nodes present in them provided effective targets for chemotherapy. Thus, in addition to providing new insights into mechanisms regulating cell cycle progression, our results also highlight that multi-module targeting - wherein the temporal dimensions of a biological process are also taken into account - may provide a useful refinement to current drug development efforts.

Downloaded from genome.cshlp.org on October 3, 2011 - Published by Cold Spring Harbor Laboratory Press

RESULTS.

An RNAi screen targeting cellular kinases and phosphatases identifies regulators of the cell cycle.

To identify signaling molecules that regulate cell cycle progression we performed a siRNA screen against all known kinases (758 proteins) and phosphatases (294 proteins) in cycling cells of the murine B lymphoma cell line CH1.This cell line has been previously used as a model system to study signaling events regulating cell cycle (Aflakian et al. 2009; Jamal et al. 2010). Changes in cell cycle phase distribution at 72h after siRNA transfection was monitored by flow cytometry (Experimental Procedures). Since our aim was to decipher processes regulating mitogen dependent cell cycle progression, only those effects that perturbed the cell cycle phases without significantly affecting cell viability were considered. A primary screen followed by a validation exercise (Fig. 1A and Supplementary Experimental Procedures), identified 38 kinases and 5 phosphatases whose silencing yielded significant effects (Supplementary Table S1). A microarray analysis subsequently confirmed that the genes coding for all of these target proteins were indeed expressed in CH1 cells (Aflakian et al. 2009)(Supplementary Table S2). A subsequent analysis using the Novoseek gene-disease relationship scores identified nearly half of these target molecules to exhibit a strong association with either one or more forms of cancer (Supplementary Fig. S3), thus emphasizing the functional relevance of the hits identified by the screen.

A hierarchical clustering analysis of the nature of effect caused by depletion of these proteins revealed that the most common one was that of a simultaneous increase in the pool size of cells resident in the G1 and S phases (Fig. 1B). In addition, there were also a significant number of cases where siRNA treatment specifically increased either the

Downloaded from genome.cshlp.org on October 3, 2011 - Published by Cold Spring Harbor Laboratory Press

G1 (12), or the S (9) phase populations, whereas only a limited number of siRNAs had any detectable affect on the G2 phase (Fig. 1B).

Silencing of signaling intermediates induces differential effects on cell doubling times.

Examination of the effects of target-specific depletion on cell population doubling times (PDTs) yielded a diverse spectrum ranging from negligible, to a marked reduction in the proliferation rate (Fig. 1C). While the PDT of control cells (i.e. transfected with non-silencing siRNA) was 26±3 h, 16 of the 43 siRNAs tested produced a significant extension with PDTs of 30h or more. The individual PDT values were then employed to calculate the residence time (RT) of cells in G1, S, and G2 phases under each of the knockdown conditions (Supplementary Experimental Procedures and Fig. S3), and these results are compared to the control value in Figure 1D. It is evident that each siRNA pool caused specific perturbations in one or more of the individual phases of the cell cycle, although the effects differed widely between the various knockdowns. For example, the G1 phase RT varied from about 2-fold lower (in 5 cases) to about 2-fold greater (in 22 cases) than that in control cells (Fig. 1D). No significant effect was observed for the remaining 16 siRNAs (Fig. 1D). A similar degree of variation was also observed for the S phase, whereas the G2 phase was only sensitive to 19 of the siRNAs tested of which 8 caused an increase in its RT (Fig. 1D).

To simplify our subsequent analysis, we categorized the target-specific siRNAs solely on the basis of the phase-specific extensions in RT that they induced (Fig. 1D). That is, although in some cases extension in RT of a given phase was compensated for by shortening of another phase, the latter effect was not taken into account. Accordingly, the largest group of siRNAs (15) corresponded to those inducing an extension of both

Downloaded from genome.cshlp.org on October 3, 2011 - Published by Cold Spring Harbor Laboratory Press

the G1 and the S phases, whereas that of only the G1 phase was observed for an additional group of 12 cases (Fig. 1D). Another set of 9 siRNAs specifically extended the S phase alone. Perturbations prolonging the G2 phase were seen in response to 4 siRNAs and the remaining three target-specific siRNAs affected either the S and G2 (2), or the G1 and G2 phases (Fig. 1D). These results are consistent with the known biological roles of these target proteins in the literature (Supplementary Table S3).

Since the role of mitogenic signals is to move cells through the G1 phase and then ensure their entry into the S phase (Jones and Kazlauskas 2000; Sears and Nevins 2002), our subsequent analysis concentrated on only those targets where depletion resulted in an extension in RT of either specifically the G1, the S, or both of these phases simultaneously. This latter group of targets was termed as those extending RT of the G1S phase and available literature suggests that it likely represents a window extending from the later stages of G1, to initiation of the S phase (Jones and Kazlauskas 2000).

Defining the source and target relationships for phase-specific regulation of the cell cycle.

An examination of results from two previously reported genome-wide screens performed in the human cell lines HeLa and U2OS (Kittler et al. 2007; Mukherji et al. 2006), revealed that there was a <5% overlap between them at the level of the signaling molecules that were identified. Relative to this, the overlap between the signaling molecules identified here and those in either of these two previous reports was between 5-10%. This poor concordance exemplifies the emerging limitations of RNAi-based screening approaches where – in addition to the preponderance of false negatives - differences in cell type and the experimental conditions employed, also significantly influence the outcome (Bushman et al. 2009; Goff 2008). It was, therefore, imperative to

Downloaded from genome.cshlp.org on October 3, 2011 - Published by Cold Spring Harbor Laboratory Press

explore whether a further interrogation of our results would yield more meaningful, and consistent, insights into signal-mediated regulation of the cell cycle.

The trade-off between sensitivity and robustness constrains the architecture of the signaling network into a bow tie - or hourglass - structure, which represents the convergence of diverse and redundant input processes onto a conserved core module or set of proteins (Csete and Doyle 2004; Supper et al. 2009). Such core elements function as the key regulators of plasticity in the cellular response, by calibrating a range of output processes (Del Sol et al.; Kitano and Oda 2006). Thus, mitogen-activated signaling networks also likely incorporate such conserved regulatory elements that process input signals, and translates them into the output response of cell cycle progression. We next attempted to reconstruct the network of pathways through which the effects of the identified targets were likely enforced.

Consequently, we defined the hits identified by our siRNA screen as ‘source nodes’ (Fig. 2A, nodes in dark red) to indicate that these signaling proteins constitute sources for inducing perturbations in the cell cycle. Further, since the effects of siRNA-mediated depletion of each of these source proteins was likely to be eventually enforced through modulations in activity of one or more constituents of the core cell cycle regulatory machinery, we considered this latter group of proteins as target nodes (Fig. 2A, light red nodes). The objective then was to trace the network of pathways connecting the sources to the targets, and search for any associated topological features (shown as green nodes linked through dotted edges) that may be central to the regulation of G1 and S phase progression. While highlighting regulatory pathways, we also anticipated that this strategy would illuminate any other key regulators that may have been missed by the screen.

Downloaded from genome.cshlp.org on October 3, 2011 - Published by Cold Spring Harbor Laboratory Press

Proteins whose depletion resulted in an extension in RT either of the G1, the S, or the G1S phases were labeled as source nodes specific for the respective phases (Fig. 2B). This was then followed by an attempt to define the putative end-targets for each of these source node groups. That is, those constituents of the core cell cycle machinery that directly influence progression of cells through the G1 or the S phases (Murray 2004). Combining literature survey with KEGG, Reactome, NCI, INOH pathway databases (Kanehisa and Goto 2000; Matthews et al. 2009; Schaefer et al. 2009) identified seventy-four such proteins, which could then be grouped either as G1 or S phase-specific 'targets' based on their known functional roles. Supplementary Table S4 lists these targets, along with links that describe evidence in support of their categorization. Due to the contiguous nature of cell cycle progression, however, it was not possible to distinguish G1S-specific targets from those involved either in the G1 or the S phases. Therefore the list of G1 and S phase targets were combined together, and taken as targets for the G1S phase.

In-silico network construction and identification of important intermediates using shortest path analysis.

Our next goal was to map the network of pathways linking the source and target nodes in each of the relevant phases. The approach employed is outlined in Figure 2C. As the first step, we consolidated the mammalian protein-protein interactions (PPI) from BIND, IntAct, HPRD, BioGRID, MINT, Reactome, and NetworKIN databases to build an undirected high confidence network consisting of 5200 nodes and 12,000 interactions (or, edges) (see Supplementary Materials and Table S5). To identify those molecular intermediates that were enriched in a cell cycle phase-specific manner (IMP nodes), we next traced all possible shortest paths from each of the classified phase-specific sources

Downloaded from genome.cshlp.org on October 3, 2011 - Published by Cold Spring Harbor Laboratory Press

(G1, S, or G1S, see Fig. 2B) to all of the corresponding phase-specific targets described in Supplementary Table S4. Shortest paths were traced from each $G1_{source}$ to all $G1_{target}$, from each S_{source} to all S_{target} and also from all $G1S_{source}$ to all $G1S_{target}$, (STEP 2, Fig. 2C).

Counting the number of times an intermediate occurred in the ensemble of shortest paths for each phase (Supplementary Table S6), and calculating the corresponding Z scores, enabled short-listing of the high scoring phase-specific IMP nodes; while normalizing for differences in the number of source and target nodes between the different cell cycle phases (STEP 2, Fig. 2C, Supplementary Experimental Procedures, and Table S6). Here, our inclusion of a G1S phase ensured that any relevant node that may potentially be involved in regulating both the G1 and S phases was not missed. This process identified 27, 22 and 32 IMP nodes from the G1, S and G1S phase-specific shortest paths respectively, and these are listed in Figure 2D.

Delineation of IMP node-dependent regulatory modules.

While the IMP nodes identified represented molecule sets that were enriched in pathways regulating the distinct cell cycle phases it was, however, important to delineate the temporal/topological regulatory features of mitogen-induced progression from G1 to S. We first took the IMP nodes from each cell cycle phase as the seed nodes, and extracted connected sub-networks of two-path length cut-off from the core network as described in Supplementary Table S5 (STEP 3 of Fig. 2C). The resulting G1 IMP node network was composed of 145 nodes and 296 edges, whereas the S IMP node network contained 54 nodes and 85 edges, with 215 nodes and 495 edges describing the G1S IMP node network (Fig. 3A-C). These sub-networks likely encapsulate the specific elements responsible for regulating the respective phases of the cell cycle.

Downloaded from genome.cshlp.org on October 3, 2011 - Published by Cold Spring Harbor Laboratory Press

To next delineate regulatory elements present in these IMP node networks, we adopted the approach outlined in STEP 3 of Figure 2C. First, a survey of the literature assisted in clarifying the nature of the biochemical reaction represented by each of the edges in the IMP node sub-networks (compiled in Supplementary Table S7). The resulting classification of these edges into functional categories of activation, inhibition (both directed), or neutral (undirected) facilitated conversion of the individual phase-specific IMP node sub-networks into mixed networks that consisted of directed and un-directed edges. Taking each of these, we then probed for any embedded motifs that also included the respective IMP nodes. Here, we employed SNAVI (Ma'ayan et al. 2009) and Figure 3D lists the various types of motifs that could be identified, and the number of times that these occurred in each of the individual phase-specific IMP node sub-networks. Integrating the phase-specific IMP node networks, and randomizing the edges while keeping the degree distribution constant over a hundred iterations led to a marked reduction in the number of motifs involving directed edges (i.e. excluding the scaffolds; Fig. 3E). This confirmed that the phase-specific motifs identified were indeed statistically significant. Further, our identification that the relative enrichment of signal-dependent regulatory motifs follows the order of G1S > G1 > S is consistent with fact that the G1/S checkpoint represents the step that is most tightly regulated by growth factor-mediated signaling (Sears and Nevins 2002; Zetterberg et al. 1995).

Extracting cell cycle regulatory modules and the identification of vulnerable nodes.

Motifs in a network do not function in isolation but, rather, integrate with one another to form discrete clusters (Dobrin 2004). In our case, such motif clusters can be considered to represent the core units that process mitogenic signals to drive the cell cycle. Therefore, we merged all motifs detected in the G1-specific IMP node network to

Downloaded from genome.cshlp.org on October 3, 2011 - Published by Cold Spring Harbor Laboratory Press

generate the G1 phase motif cluster. Similarly, motifs present in the G1S- or the S-specific IMP node networks were also independently merged to generate motif clusters defining the regulation of corresponding phases. Importantly, these motif clusters exhibited a high degree of edge density when compared to random sub-networks extracted from IMP node networks (see Supplementary Materials). Thus, these phase-specific motif clusters likely define regulatory modules that specifically function during the cell cycle phases from which they were derived. A compilation of the nodes present in these modules, along with a classification of the functional groups to which they belong, is provided in Supplementary Table S8.

Having extracted the cell cycle phase-specific regulatory modules, we next sought to identify those constituent nodes that were most critical for their functioning. For this we employed the centrality measures of 'stress' and 'betweenness'. Stress and betweenness represent complementary indices that together describe the functional importance of a node in a regulatory module (Manimaran et al. 2009; Newman 2005). We calculated the stress and betweenness measures for each node in each phase-specific module, and the resulting plot of these values for the G1 and G1S specific modules is shown in Figure 4A. Here, as expected, the S-specific module was comprised of only a few nodes (see Supplementary Table S8) with just two giving any measurable value for stress and betweenness. The modules for the G1, G1S, and S phases are shown in Figures 4B-D, where the nodes are color-coded according to their stress and betweenness values. The larger the size of the node the higher is the respective value of stress, whereas the betweenness value is indicated by the shade of the color for that node.

We next segregated the functionally most significant nodes as those with stress and betweenness values that were both greater than 2.5-fold that of the mean for all nodes in the corresponding module (Supplementary Experimental Procedures, Fig. 4A). The

Downloaded from genome.cshlp.org on October 3, 2011 - Published by Cold Spring Harbor Laboratory Press

composition of the resulting shortlist was then compared across the individual phases. Intriguingly, the high stress and high betweenness nodes identified for the G1, G1S, and S windows of the cell cycle did not constitute distinct sets of molecules. Rather, the group of vulnerable nodes identified for a given window overlapped significantly with that for the adjacent window. For example, while PTK2B was exclusively present in the G1 module ESR1, SRC, and GRB2 commonly occurred as high-stress and high-betweenness nodes in both G1 and G1S modules (Fig. 4A). Interestingly, although AKT1 and E2F1 were also present in both modules (Supplementary Table S8), these proteins exhibited properties of high stress and betweenness only in the context of the G1 module (see Fig. 4 A-C). The nodes exclusively present in the G1S module were ABL1, JUN, BRCA1, EP300, and RB1 (Fig. 4A). In the S module, only CCNA2 and RBL1 showed functional non-redundancy (i.e. high stress and betweenness, Fig. 4D). The observed overlap in structure between modules describing the adjacent windows of the cell cycle is consistent with the fact that individual stages of this process do not represent discrete events, but rather reflect windows that capture temporally defined stages of a contiguously evolving biochemical cascade.

Interestingly the majority of the G1-unique nodes represented signaling molecules, whereas nodes specific for the G1S IMP node network were distributed between signaling molecules, transcription regulators, and proteins involved in DNA replication (Supplementary Table S8). The nodes enriched in S phase network included CDK2 and CCNA2, which form a complex that drives cells through the S phase (Arias and Walter 2007). Other such enriched nodes included here were the damage repair protein BRCA1, the DNA replication factor RIS2, and RBL1 – a key regulator of entry into cell division (Harper and Elledge 2007). Figure 4E summarizes the distinct classes of biochemical activities described by each of the IMP node sub-networks in the form of a heat map.

Downloaded from genome.cshlp.org on October 3, 2011 - Published by Cold Spring Harbor Laboratory Press

The observed layering of the initial activation of signaling events (G1 and G1S) over the overlapping phase involving the induction of transcriptional processes (G1S), and subsequent recruitment of the DNA replication machinery (G1S and S) accurately recapitulates the broad sequence of events that govern cell cycle progression.

These collective results, therefore, substantiate the information-rich nature of the IMP node modules shown in Figure 4. They also support that these modules together capture the dynamic transitions in biochemical activities that enforce commitment of cells to the division cycle.

Verifying phase-specificity of vulnerable nodes.

To further validate relevance of the phase-specific modules, we experimentally verified both the selection of high-stress high-betweenness nodes, and the characterization of their phase-specificity. We first compared between the effects obtained upon perturbation either of AKT or ABL. Our IMP node modules had suggested that the functional significance of AKT1 was restricted to the G1-specific module whereas ABL1 was specific to the G1S module. Therefore, we treated CH1 cells with pharmacological agents that either inhibited AKT phosphorylation (LY294002), or, ABL activity (Imatinib mesylate). The concentration of both inhibitors was adjusted such that a similar PDT was obtained in both cases, thereby enabling a direct comparison between the RT of the individual phases. Inhibition of AKT resulted in a specific extension of the G1 phase, with a marginal reduction in RT of the S phase of the cycle (Fig. 5A). In contrast, the increased PDT obtained upon ABL inhibition involved contributions from both the G1 and S phases (Fig. 5A). These results therefore verify the distinctions in phase-specificity that were earlier suggested for these two nodes, on the basis of centrality index estimations.

Downloaded from genome.cshlp.org on October 3, 2011 - Published by Cold Spring Harbor Laboratory Press

We also tested the effects of perturbing the remaining high-stress, high-betweenness nodes that were identified (Fig. 5B). As earlier discussed, the large majority of high-stress high-betweenness nodes identified were those that were either unique to G1S, or shared between the G1 and G1S modules. Consistent with this, perturbation at any of these nodes resulted in a simultaneous increase in RT of both the G1 and the S phase (Fig. 5B). However, RT of the G2 phase was unaffected. Further, in line with our identification of this protein as a G1-specific regulatory factor, silencing of PTK2B led to a biased extension of the G1 phase (Fig. 5B). The only discrepant result obtained was for E2F1 whose silencing perturbed both the G1 and S phases, although this protein was characterized as a node whose vulnerability was restricted to the G1 phase (Fig. 4A). This, however, may not be surprising given that the downstream products of E2F-dependent transcriptional regulation (e.g. cyclins A, B and E) drive both the later stages of G1, as well as the S phase of the cycle.

Finally, with the exception of CDK5, silencing of nodes with low values for stress and betweenness (i.e. < 1.5 fold of the mean value) had no significant effect on phase-specific RTs. Although CDK5 is suspected to play a role in cell cycle regulation, its properties and function have been less explored (Dhavan and Tsai 2001). This may account for the lesser number of associations known for CDK5 and, thereby, the resulting low values for stress and betweenness. Thus, the results in Figure 5A and B provide experimental support for the functional description of nodes, on the basis of centrality indices, from the corresponding regulatory modules. However, they also underscore the possibility that some additional critical nodes may have been missed either due to insufficient information, or noise in the curated PPI databases.

Downloaded from genome.cshlp.org on October 3, 2011 - Published by Cold Spring Harbor Laboratory Press

High stress, high betweenness nodes represent vulnerable constituents of phase-specific regulatory modules.

The identification of critical nodes on the basis of centrality measures also implied that these were the functionally least redundant, or most vulnerable, nodes within the respective cell cycle phase-specific modules. Consequently, inactivation of one or more of these nodes should then exert a profound influence on the cell cycle. Consistent with this, treatment of CH1 cells with an inhibitor of either AKT1 activation, or that of ABL1 activity resulted in a dose-dependent increase in the frequency of apoptotic cells (Fig. 5C). Importantly, this apoptotic response was preceded by an accumulation of cells in the G1 phase (Fig. 5D), confirming that cell death derived from an arrest in the cycle. Here, for the purposes of comparison, we also examined the effects of inhibition of five representative target proteins that had been identified by our siRNA screen (Fig. 1). Of these, two (CHEK1 and FGFR2) represented G1-specific source nodes and the remaining three (TRPM7, PRKAR1A and MET) were G1S source nodes (see Fig. 2B). Whereas inhibitors of CHEK1 and TRPM7 were significantly less potent than that of AKT1 and ABL1, only marginal effects were obtained upon either PRKAR1A, FGFR2, or MET inhibition (Fig. 5C). The inhibitors used in these experiments, along with the IC_{50} values for their respective targets, are listed in Figure 5E.

Our interpretation that the vulnerable character of AKT1 and ABL1 emerged in temporally distinct windows of the cell cycle regulatory module also implied that simultaneous inhibition of both AKT1 and ABL1 should produce a cooperative effect on cell cycle arrest, and the consequent apoptosis. This expectation was indeed borne out in a subsequent experiment (Fig. 5F), and the Loewe Combination Index (CI) obtained was 0.56 ± 0.08. Here, a CI of <1 is indicative of a synergistic response (Chou and Talalay 1981). In contrast, apoptosis induction by combinations of inhibitors of either CHEK1

Downloaded from genome.cshlp.org on October 3, 2011 - Published by Cold Spring Harbor Laboratory Press

or FGFR2 (G1-specific source nodes) with that of TRPM7, PRKAR1A, or MET (G1S-specific source nodes) was poor (Fig. 5F). Thus, the cumulative results in Figure 5C and F confirm that both AKT and ABL exhibit a degree of vulnerability that is significantly greater than at least some of the targets identified in our siRNA screen. This however, does not rule out the possibility that there may be other combinations not tested in this study, which may also be effective. Further, the cooperative effects of combined inhibition observed also supports our inferred distinction in phase-specific involvement (G1 versus G1S) of at least two of the nodes (AKT1 and ABL1) identified on the basis of centrality indices.

IMP node modules define the signaling axes that govern G1 and G1S windows of the cell cycle.

The extraction of the G1 and G1S IMP node modules also helped to resolve the nature of receptor-proximal signals that govern commitment of cells to the division cycle. In the G1 IMP node module, four molecules likely represent key constituents of the signaling cascade that governs the early G1. While AKT1 and PTK2B play a more specific role in this process, SRC and the adaptor molecule GRB2 represent the least redundant constituents of both G1 and G1S modules (Fig. 4). SRC likely serves as a common sensor that bridges AKT1 activation with both RTKs and mitogenic GPCRs. Whereas the SRC/GRB2 complex represents a constituent of the signalosome complex recruited by RTKs (Luttrell and Luttrell 2004), PTK2B mediates SRC activation by GPCRs (Litvak et al. 2000). This may then explain earlier observations that distinct mitogenic signals activate a common signaling cascade in the early G1 response (Jones and Kazlauskas 2001).

Downloaded from genome.cshlp.org on October 3, 2011 - Published by Cold Spring Harbor Laboratory Press

ABL1 was the unique kinase present as a high-stress high-betweenness node in the G1S IMP node network (Fig.4). While its inferred functional significance was experimentally verified (Fig. 5A), earlier studies have also demonstrated that depletion in levels of ABL1 significantly delays entry of cells into the S phase (Furstoss et al. 2002). Similar to AKT1, activation of ABL1 is also primarily dependent upon the upstream SRC, which occurs both through direct and indirect mechanisms (Plattner et al. 1999; Sirvent et al. 2008). Thus, the early G1 is likely regulated through the complement of pathways initiated by the SRC-AKT1 signaling axis. Continuance through late G1, and then entry into the S phase, however appears to be contingent upon a switch in this axis where ABL1 now replaces AKT1 as the non-redundant substrate of SRC (see Fig. 6 inset).

IMP node modules capture the network of core pathways that mediate commitment of cells to the division cycle.

To translate our delineation of the distinct receptor-proximal signals into a more coherent view of G1 and G1S phase regulation, we merged the corresponding IMP node modules and extracted the motifs incorporating the combined list of high-stress high-betweenness nodes. By then enriching the resulting links with information from the literature, we transformed these into the pathway map shown in Figure 6. It is evident that this map represents a synopsis of the multiplicity of biochemical events that cumulatively drive commitment of cells to the division cycle. Importantly it also elaborates the individual modes of functioning of the G1- and G1S-specific signaling cascades, as well as the links between them that coordinate their respective activities.

The analysis reiterates that AKT1-dependent pathways indeed initiate cell cycle progression, by a concomitant inhibition of pro-apoptotic pathways being coordinated

Downloaded from genome.cshlp.org on October 3, 2011 - Published by Cold Spring Harbor Laboratory Press

with mechanisms regulating cell growth and proliferation (Fig. 6). Similarly, this figure also rationalizes the key role ascribed to ABL1 in regulation of late G1 and the subsequent G1/S transition. As shown, pathways emanating from the cytoplasmic pool of ABL1 influence both cell cycle progression and also suppress pro-apoptotic mechanisms (Fig.6). A prominent downstream consequence of cytoplasmic ABL1 activation is the enhancement in levels of cellular c-MYC (Boureux et al. 2005), the central regulator that links external signals to the cell cycle machinery (Obaya et al. 1999). Importantly, the cell cycle regulatory effects of MYC predominantly impinge on the later stages of G1, and facilitate entry of cells into the S phase (Heikkila et al. 1987; Santoni-Rugiu et al. 2000).

Release of the nuclear-localized ABL1 from its inhibitory complex with RB, which occurs as cells approach the G1/S boundary (Welch and Wang 1995), also contributes towards regulating MYC levels. The resulting convergence in signaling pathways, initiated from both the cytoplasmic and nuclear pools of ABL1, may well explain the long-standing question of how cellular MYC levels are temporally modulated during cell cycle progression. While expression of this protein is induced in the early G1 phase, these levels are further enhanced as cells prepare for S phase entry (Jones and Kazlauskas 2001). Interestingly, consistent with our proposal, the timing of this second phase of MYC enhancement coincides with that of dissociation of the RB-ABL complex (Welch and Wang 1993). Synergism between the cytoplasmic and nuclear pools of ABL may therefore provide a plausible mechanism that enables ABL1 to replace AKT1 as the dominant signaling node in the G1S phase. This effect is likely augmented by the fact that, subsequent to its release from RB, a fraction of the nuclear ABL also partitions into the cytoplasmic compartment (di Bari et al. 2006). The resulting increase in the pool of cytoplasmic ABL1 would then further intensify signals generated from this subset of the

Downloaded from genome.cshlp.org on October 3, 2011 - Published by Cold Spring Harbor Laboratory Press

kinase. Significantly, our proposal that ABL1-dependent signaling is markedly amplified as cells approach the G1/S boundary is well supported by recent findings that cellular levels of phosphorylated ABL1 peak at the G1S phase (Olsen et al. 2010).

These cumulative results therefore rationalize our assignment of key, but distinct, regulatory roles to AKT1 and ABL1 in the early and late G1 stages respectively. The MAP kinase pathway likely serves as a common link that facilitates transition between these two phases. Thus, in addition to delineating the key receptor-proximal molecules, the results of our graph theoretical analysis also facilitated synthesis of existing – albeit piecemeal - data into a more unified scheme. This scheme captures the temporal evolution of signaling cascades, as they propel cells through the mitogen-sensitive phase of the cycle.

A comparative analysis of independently conducted screens yields a common IMP node network.

Since cell cycle regulation is common to all dividing cells, it would be reasonable to expect that the core modules identified here - and the IMP node network from which they were extracted - would represent a common feature of dividing cells, independent of their tissue type of origin. To verify this, we also analyzed results of the previously described RNAi-based screens for cell cycle regulators that were performed in HeLa and U2OS cells (Kittler et al. 2007; Mukherji et al. 2006). As noted earlier, the overlap in signaling molecules identified between these two screens was <5%.

From each of these reports we separately shortlisted the signaling molecules described as ‘hits’ for either the G1 or S phase (the G1S phase was not characterized in these studies), and categorized them as G1+S source nodes. We next repeated the analysis described in Figure 2A wherein shortest paths were traced from each of these

Downloaded from genome.cshlp.org on October 3, 2011 - Published by Cold Spring Harbor Laboratory Press

source nodes, to each of the G1+S target nodes described earlier. By then subtracting against the corresponding G2-specific source to target network, we extracted the IMP nodes as described in Figure 2C. A similar exercise was also performed with the results of our present screen, which then allowed us to compare the resulting IMP node list with that obtained from the HeLa and U2OS cell screens. Remarkably, in spite of the nominal degree of concordance at the level of the RNAi-defined hits, there was a >70% overlap in the IMP nodes derived from the three screens (Supplementary Fig. S5). Further, when IMP node networks were independently generated from each of these three lists, the resulting overlap between them was >92% (Supplementary Fig. S5).

To rule out any potential bias that our procedure for identifying IMP nodes may only detect highly connected proteins, we performed validation exercises at two levels. First, three different random pairs of protein sources and targets were sampled from the core PPI network, and IMP nodes were identified with respect to this background. The resulting overlap between three random source-target nodes (<30%; Supplementary Fig. S5) was significantly less than the 70% value observed in our comparison between IMP nodes from the three studies. Second, to assess for any bias resulting from the employment of a common set of target nodes, we sampled random set of sources from the core PPI network while retaining the targets (i.e. cell cycle targets, Table S4). The overlap in IMP nodes identified from this exercise was about 40% (Fig. S5). Thus any random set of source when employed with the same cell cycle targets does not identify a conserved set of IMP nodes. Finally, the overlap between our CH1 IMP nodes and the three sets of random IMP nodes was less than 38% (Fig. S5), further confirming that the observed overlap in IMP nodes between the three independent screens obtained with the two other independent RNAi screen results was indeed significant and not a random or biased event.

Downloaded from genome.cshlp.org on October 3, 2011 - Published by Cold Spring Harbor Laboratory Press

These cumulative findings thus establish the significance of our methodology for further interrogating the siRNA screen results. In addition, they also support the likelihood that the IMP nodules identified from our data constitute conserved regulatory elements of the mitogen-dependent signaling network.

The G1 and G1S IMP node modules represent conserved elements of mitogen-activated signaling cascades.

To experimentally verify our above inference that the delineated IMP node modules may constitute invariant features that are common to all dividing cells we took a panel of fourteen human cell lines derived from a diverse range of tissue types (see Supplementary Figure S6B). These cells were treated with a single dose of either the combined inhibitors of AKT and ABL or, for purposes of comparison, combinations of inhibitors against the siRNA-identified targets (C1, C2, and C3 in Fig. 4F). The frequency of apoptotic cells obtained in each case was then determined 48h later and the results are presented in Figure 7A. The efficacy of the inhibitor combinations C1, C2, and C3 was highly restricted with the combination C2 inducing significant (i.e. >30%) apoptosis only in four of the cell lines tested. Further, with the exception of Jurkat cells, effects on the remaining cell lines were predominantly due to CHEK1 inhibition with little or no contribution from PKA inhibition (Supplementary Fig. S6). This was also true of the effects of combination C1 on THP1 and U937 cells, whereas the combination C3 was virtually ineffective (Fig. 7A).

In contrast to these limited effects, simultaneous inhibition of AKT and ABL induced significant levels of apoptosis in all the cell lines tested, which also included HeLa and U2OS cells (Fig. 7A). This effect was further enhanced by the 72h time point where the number of apoptotic cells was >80% in all cases. These findings, therefore, further

Downloaded from genome.cshlp.org on October 3, 2011 - Published by Cold Spring Harbor Laboratory Press

support the functional distinction between at least the hits from the siRNA screen tested here, and the high vulnerability nodes identified from a graph theoretical derivation of the phase-specific regulatory modules. That is, in comparison with the former group the latter represents nodes that are involved in a less redundant manner, during cell cycle regulation of a broader range of cancer cell types. Notably, none of the inhibitor combinations examined had any significant affect on viability of normal B-lymphocytes purified from the peripheral blood of six different individuals (Fig. 7B). This confirms that the functional relevance of AKT1 and ABL1 is only expressed in actively cycling cells.

To assess whether responses to the combined inhibition of ABL and AKT in Figure 7A were synergistic we determined the CI values from dose-response curves either to LY294002, Imatinib mesylate, or the combination of both in each instance. Figure 7C shows clear evidence for a synergistic effect in twelve of the fourteen cell lines. Importantly, this also included examples where either one (Imatinib mesylate in Namalwa and THP1 cells), or both inhibitors (Jurkat and A549 cells) had no significant effect on cell survival when administered individually (Fig. 7D); further emphasizing the extent of cooperativity achieved by the inhibitor combination in these cells. For the remaining two cell lines however (HEK293 and HEPG2), combined inhibition of both ABL and AKT yielded an outcome that was only additive in nature. We reasoned that this absence of synergy for the inhibitor combination in these latter two cell lines could derive from subtle, cell type-inherent, differences in the architecture of the IMP node modules. This could then influence the degree of vulnerability exhibited by AKT1 and ABL1. Consequently, we probed this latter group further by also including SRC inhibitor PP1a, along with those for ABL and AKT. As earlier discussed, SRC

Downloaded from genome.cshlp.org on October 3, 2011 - Published by Cold Spring Harbor Laboratory Press

principally functions by mediating either AKT1 activation in the G1 phase, or ABL1 activation in the G1S phase.

Figure 7E shows that although SRC inhibition alone had no significant effect on either of the cell lines tested, a strong synergistic effect was nonetheless obtained when it was combined with the inhibitors of both AKT and ABL. Thus, by combining SRC inhibition along with that for AKT1 and ABL1, it seems possible to also guard against any cell type-specific variations in topology of the G1 and G1S IMP node modules. Important here is that in all cases involving inhibition of vulnerable nodes - or their combinations - in Figure 7, increased apoptosis was always preceded by an accumulation of cells in the G1 phase, supporting that cell death was indeed mediated through an arrest in the cell cycle. These cumulative results, therefore, confirm that the G1 and G1S IMP node modules described in Figure 4 indeed represent signal processing elements that commonly mediate cell cycle progression in at least a wide range of cell types. Further, the vulnerable nodes that they incorporate provide sensitive targets for achieving an efficient disruption of the cell cycle regulatory network.

Downloaded from genome.cshlp.org on October 3, 2011 - Published by Cold Spring Harbor Laboratory Press

DISCUSSION.

RNAi-based screens are now being commonly employed to probe a wide variety of biological processes. Recent results, however, have begun to highlight limitations inherent to this approach. Prominent among these are the preponderance of false negatives, and the highly cell type-restricted nature of the results obtained (Bushman et al. 2009). Consequently, the poor convergence between results from different laboratories often hampers the extraction of any meaningful interpretation. It was for this reason that we were prompted to explore graph theoretical approaches for unraveling the mechanistic implications of the hits identified in our screen. Previous studies support the utility of analyzing network interactions in receptor-specific pathways, to generate insights into signaling mechanisms. Further, they also emphasized the potential of this approach for identifying new drug targets (Astsaturov et al. 2010; Bandyopadhyay et al. 2010; Tu et al. 2009).

Central to our analysis was the identification of phase-specific IMP nodes, which were selected on the basis of their unique over-representation in each of the phase-specific regulatory sub-networks. These IMP nodes likely combine the traits of minimal functional redundancy and increased specificity of action, in the context of regulation of the respective window of the cell cycle. By extension then, the modules defined by the phase-specific group of IMP nodes also likely constitute the key regulatory elements that process mitogenic (and oncogenic?) signals for the corresponding cell cycle phases. Here, a re-examination of data from the two previously described screens validated both the relevance and significance of our approach. The virtually similar IMP node network that was extracted in all cases also lent preliminary support to our proposition of the existence of a conserved set of core elements that regulate mitogenic signals.

Downloaded from genome.cshlp.org on October 3, 2011 - Published by Cold Spring Harbor Laboratory Press

Examination of the incorporated links revealed novel details on the mode of functioning of these modules. For instance, the G1 and G1S modules both participate in the critical function of coordinating cell cycle progression with cell growth, in a setting where pro-apoptotic pathways are inhibited. The shared activities between the individual modules maintains contiguity during progression of cells from early G1 up to the S phase, whereas integration between the three modules promotes temporal evolution of the spectrum of biochemical processes that drive commitment of cells to the cycle. Particularly significant here was our discovery that the G1 and G1S phases were controlled by distinct signaling axes that were composed of SRC-AKT and SRC-ABL respectively. Further, we also subsequently elucidated that it was the switch between these two axes that guided transition of cells from early to late G1/G1S.

In addition to defining the receptor-proximal signals, however, our cumulative results further established that the IMP node modules in fact also capture the key regulatory elements that translate the effector consequences of mitogenic/oncogenic signaling to the respective stages of the cell cycle. In this connection, our experiments demonstrating that these cumulative functional properties of the G1 and G1S modules were conserved across a diverse panel cell lines is particularly significant. That is, these phase-specific modules presumably describe core information-processing units of the mitogen-activated signaling network, which function - in at least a broad range of cell types - to ensure irreversible commitment to the cycle. Future studies on the systems properties of these modules may provide important clues on mechanisms underlying cell transformation, and also on factors that govern properties related to cellular growth rate such as tumor aggressiveness and metastasis.

The identification of IMP node modules and delineation of their vulnerable constituents also facilitated the exploration of a potentially more effective strategy for

Downloaded from genome.cshlp.org on October 3, 2011 - Published by Cold Spring Harbor Laboratory Press

chemotherapy. In view of the pathway redundancies that are inherent to signaling networks, current emphasis is on approaches that involve a concerted pharmacological intervention at multiple key targets (Lehar et al. 2008b). The challenge, however, is to identify the most appropriate combination of nodes to be targeted, and present approaches in this direction are limited by the vast space of high-order combinations that are theoretically possible (Lehar et al. 2008a). Here, our present strategy of extracting vulnerable nodes from the core elements that process input signals in a context-specific manner, alone serves to reduce the dimensions of combination space to be explored by several orders of magnitude. Further, as we have demonstrated, the relative functional conservation of these regulatory elements also implies that the benefits of targeting such nodes would be at least less cell type-restricted.

From a broader point of view, the above results also support that targeting nodes derived from modules that regulate temporally distinct stages provides for a more effective means for breaching the fragility barrier of the cell cycle regulatory network. That is, these findings emphasize the potential of exploiting the temporal dimensions of a biological process, an aspect that is presently ignored in ongoing drug development exercises. At one level, targeting combinations of nodes whose functional vulnerabilities are conserved can potentially override current limitations faced due to problems of cell- and tissue-type heterogeneity. In addition, the observed synergism between AKT1 and ABL1 inhibition also entails a broader therapeutic window, thus providing an advantage over several of the chemotherapeutic agents currently in use (Kaelin 2005). Our proposal is particularly well supported by emerging evidence that a role for constitutive ABL activity is not restricted to CML alone but, rather, is now implicated in a broader spectrum of cancers (Sirvent et al. 2008). This would be consistent with our present description of ABL1 as the key regulatory signaling molecule that drives the G1S phase.

Downloaded from genome.cshlp.org on October 3, 2011 - Published by Cold Spring Harbor Laboratory Press

Also to be noted in this context is the possibility of exploiting the other vulnerable nodes that were identified in the individual IMP node modules, through the development of specific inhibitors.

Thus, in summary, our present report describes an integration of results from a siRNA screen with graph theoretical analysis, to delineate the core signaling modules that regulate the early phases of the cell cycle. Importantly, these modules could be demonstrated to represent elements that were conserved across a broad range of cell types, and could be exploited for elaborating novel mechanistic features pertaining to signal-mediated regulation of the cell cycle. Notable among these was the delineation of the distinct core signaling axes that governed early and late G1 phases, and subsequent elucidation of the seamless manner in which the switch between them was integrated. Further, successful resolution of the least redundant nodes in each of the regulatory modules also permitted the development of a strategy for multi-module targeting in order to achieve synergistic disruption of the cell cycle. These latter findings thus pave the way for overcoming the daunting challenge presently faced, in identifying target combinations that can yield synthetic lethal effects in mammalian cells (Kaelin 2005; Kaelin 2009).

Downloaded from genome.cshlp.org on October 3, 2011 - Published by Cold Spring Harbor Laboratory Press

EXPERIMENTAL PROCEDURES.

Materials.

All cell lines used in this study were originally procured from the American Tissue Culture Collection with the exception of AW8507, which was obtained from Dr. Shubha Chiplunkar (ACTREC, Navi Mumbai). Normal B-lymphocytes were purified from the blood of donors by using the B-cell negative selection kit from Dynal and following the protocol recommended by the manufacturer. Purity of these cells were >90% as assessed by CD19 staining. Antibodies were purchased from Cell Signaling Technologies. For the primary screen, siRNAs were obtained from Qiagen whereas for the validation screen they were obtained either from Sigma Chemical Co. (for Kinases) or from Dharmacon Inc. (for phosphatases). Further details of these are provided in Supplementary experimental procedures. All chemical inhibitors used here were purchased from Tocris Biosciences except for Imatinib mesylate, which was obtained as a gift from Sundeep Dugar (Sphaera Pharma).

siRNA screen.

Details of the standardization of conditions for the siRNA screen, the protocol adopted, and the data analysis procedures are provided in Supplemental Experimental Procedures. Briefly, CH1 cells were seeded in wells of a 96-well plate at 2 x 10^4/well and transfected, in duplicate, either with control, or, target-specific siRNA. At 72h later these cells were stained with propidium iodide and analyzed for the DNA content by flow cytometry. An analysis of the results using the FlowJo software yielded the DNA histograms for quantification of the sub-G1, G1, S, and G2 populations. The Z-scores for each parameter were then calculated by employing the corresponding mean values, and the standard deviations, of the five negative controls in each plate as described in

Downloaded from genome.cshlp.org on October 3, 2011 - Published by Cold Spring Harbor Laboratory Press

Supplemental Experimental Procedures. Short-listed hits were then taken for further validation as described in the text. By using various criteria, we also confirmed that our screen was robust, reproducible, and sensitive with an overall z-factor of 0.56 (see Supplementary Experimental Procedures). Determination of the effect of siRNA treatment on the population doubling time and the consequent estimation of phase-specific RTs is also described in detail in Supplementary Experimental Procedures.

Network analyses.

An outline of the approach is described Figure 2C. A step-by-step description of the graph theoretical approaches for arriving at the IMP node networks and – eventually – the vulnerable nodes is provided in Supplementary Experimental Procedures.

Downloaded from genome.cshlp.org on October 3, 2011 - Published by Cold Spring Harbor Laboratory Press

ACKNOWLEDGEMENTS.

This work was supported by a grant (to K.V.S.R) from the Department of Biotechnology, Govt. of India. NJ and SR are recipients of a Senior Research Fellowship from the CSIR and SRH received a Senior Research Fellowship from the UGC. We thank Shubha Chiplunkar (ACTREC) and Ramesh Bamezai (JNU) for gifts of the AW8507 and MCF7 cells respectively.

CONTRIBUTIONS.

N.J and K.V.S.R managed the project. S.R, S.R.H, S.C.M and N.J performed the network and screen analysis. N.J and Z.S performed the experiments. N.J, S.R and K.V.S.R interpreted results and wrote the manuscript.

Downloaded from genome.cshlp.org on October 3, 2011 - Published by Cold Spring Harbor Laboratory Press

REFERENCES.

Aflakian, N., S. Ravichandran, M.S. Jamal, H. Jarvenpaa, R. Lahesmaa, and K.V. Rao. 2009. Integration of signals from the B-cell antigen receptor and the IL-4 receptor leads to a cooperative shift in the cellular response axis. *Mol Biosyst* **5:** 1661-1671.

Alon, U. 2007. Network motifs: theory and experimental approaches. *Nat Rev Genet* **8:** 450-461.

Astsaturov, I., V. Ratushny, A. Sukhanova, M.B. Einarson, T. Bagnyukova, Y. Zhou, K. Devarajan, J.S. Silverman, N. Tikhmyanova, N. Skobeleva, A. Pecherskaya, R.E. Nasto, C. Sharma, S.A. Jablonski, I.G. Serebriiskii, L.M. Weiner, and E.A. Golemis. 2010. Synthetic lethal screen of an EGFR-centered network to improve targeted therapies. *Sci Signal* **3:** ra67.

Bandyopadhyay, S., C.Y. Chiang, J. Srivastava, M. Gersten, S. White, R. Bell, C. Kurschner, C.H. Martin, M. Smoot, S. Sahasrabudhe, D.L. Barber, S.K. Chanda, and T. Ideker. 2010. A human MAP kinase interactome. *Nat Methods* **7:** 801-805.

Barabasi, A.L. and Z.N. Oltvai. 2004. Network biology: understanding the cell's functional organization. *Nat Rev Genet* **5:** 101-113.

Boureux, A., O. Furstoss, V. Simon, and S. Roche. 2005. Abl tyrosine kinase regulates a Rac/JNK and a Rac/Nox pathway for DNA synthesis and Myc expression induced by growth factors. *J Cell Sci* **118:** 3717-3726.

Bushman, F.D., N. Malani, J. Fernandes, I. D'Orso, G. Cagney, T.L. Diamond, H. Zhou, D.J. Hazuda, A.S. Espeseth, R. Konig, S. Bandyopadhyay, T. Ideker, S.P. Goff, N.J. Krogan, A.D. Frankel, J.A. Young, and S.K. Chanda. 2009. Host cell factors in HIV replication: meta-analysis of genome-wide studies. *PLoS Pathog* **5:** e1000437.

Chou, T.C. and P. Talalay. 1981. Generalized equations for the analysis of inhibitions of Michaelis-Menten and higher-order kinetic systems with two or more mutually exclusive and nonexclusive inhibitors. *Eur J Biochem* **115:** 207-216.

Del Sol, A., R. Balling, L. Hood, and D. Galas. 2010. Diseases as network perturbations. *Curr Opin Biotechnol* **21:** 566-571.

Dhavan, R. and L.H. Tsai. 2001. A decade of CDK5. *Nat Rev Mol Cell Biol* **2:** 749-759.

di Bari, M.G., L. Ciuffini, M. Mingardi, R. Testi, S. Soddu, and D. Barila. 2006. c-Abl acetylation by histone acetyltransferases regulates its nuclear-cytoplasmic localization. *EMBO Rep* **7:** 727-733.

Dobrin, R., Q.K. Beg, A.L. Barabási and Z.N. Oltvai. 2004. Aggregation of topological motifs in the Escherichia coli transcriptional regulatory networks. *BMC Bioinformatics* **5**.

Edelman, G.M. and J.A. Gally. 2001. Degeneracy and complexity in biological systems. *Proc Natl Acad Sci U S A* **98:** 13763-13768.

Evan, G.I. and K.H. Vousden. 2001. Proliferation, cell cycle and apoptosis in cancer. *Nature* **411:** 342-348.

Furstoss, O., K. Dorey, V. Simon, D. Barila, G. Superti-Furga, and S. Roche. 2002. c-Abl is an effector of Src for growth factor-induced c-myc expression and DNA synthesis. *Embo J* **21:** 514-524.

Goff, S.P. 2008. Knockdown screens to knockout HIV-1. *Cell* **135:** 417-420.

Harper, J.W. and S.J. Elledge. 2007. The DNA damage response: ten years after. *Mol Cell* **28:** 739-745.

Downloaded from genome.cshlp.org on October 3, 2011 - Published by Cold Spring Harbor Laboratory Press

Heikkila, R., G. Schwab, E. Wickstrom, S.L. Loke, D.H. Pluznik, R. Watt, and L.M. Neckers. 1987. A c-myc antisense oligodeoxynucleotide inhibits entry into S phase but not progress from G0 to G1. *Nature* **328:** 445-449.

Jamal, M.S., S. Ravichandran, N. Jailkhani, S. Chatterjee, R. Dua, and K.V. Rao. 2010. Defining the antigen receptor-dependent regulatory network that induces arrest of cycling immature B-lymphocytes. *BMC Syst Biol* **4:** 169.

Jones, S.M. and A. Kazlauskas. 2000. Connecting signaling and cell cycle progression in growth factor-stimulated cells. *Oncogene* **19:** 5558-5567.

Jones, S.M. and A. Kazlauskas. 2001. Growth-factor-dependent mitogenesis requires two distinct phases of signalling. *Nat Cell Biol* **3:** 165-172.

Kaelin, W.G., Jr. 2005. The concept of synthetic lethality in the context of anticancer therapy. *Nat Rev Cancer* **5:** 689-698.

Kaelin, W.G., Jr. 2009. Synthetic lethality: a framework for the development of wiser cancer therapeutics. *Genome Med* **1:** 99.

Kanehisa, M. and S. Goto. 2000. KEGG: kyoto encyclopedia of genes and genomes. *Nucleic Acids Res* **28:** 27-30.

Kittler, R., L. Pelletier, A.K. Heninger, M. Slabicki, M. Theis, L. Miroslaw, I. Poser, S. Lawo, H. Grabner, K. Kozak, J. Wagner, V. Surendranath, C. Richter, W. Bowen, A.L. Jackson, B. Habermann, A.A. Hyman, and F. Buchholz. 2007. Genome-scale RNAi profiling of cell division in human tissue culture cells. *Nat Cell Biol* **9:** 1401-1412.

Lehar, J., A. Krueger, G. Zimmermann, and A. Borisy. 2008a. High-order combination effects and biological robustness. *Mol Syst Biol* **4:** 215.

Lehar, J., B.R. Stockwell, G. Giaever, and C. Nislow. 2008b. Combination chemical genetics. *Nat Chem Biol* **4:** 674-681.

Litvak, V., D. Tian, Y.D. Shaul, and S. Lev. 2000. Targeting of PYK2 to focal adhesions as a cellular mechanism for convergence between integrins and G protein-coupled receptor signaling cascades. *J Biol Chem* **275:** 32736-32746.

Luttrell, D.K. and L.M. Luttrell. 2004. Not so strange bedfellows: G-protein-coupled receptors and Src family kinases. *Oncogene* **23:** 7969-7978.

Ma'ayan, A., S.L. Jenkins, R.L. Webb, S.I. Berger, S.P. Purushothaman, N.S. Abul-Husn, J.M. Posner, T. Flores, and R. Iyengar. 2009. SNAVI: Desktop application for analysis and visualization of large-scale signaling networks. *BMC Syst Biol* **3:** 10.

Manimaran, P., S.R. Hegde, and S.C. Mande. 2009. Prediction of conditional gene essentiality through graph theoretical analysis of genome-wide functional linkages. *Mol Biosyst*.

Matthews, L., G. Gopinath, M. Gillespie, M. Caudy, D. Croft, B. de Bono, P. Garapati, J. Hemish, H. Hermjakob, B. Jassal, A. Kanapin, S. Lewis, S. Mahajan, B. May, E. Schmidt, I. Vastrik, G. Wu, E. Birney, L. Stein, and P. D'Eustachio. 2009. Reactome knowledgebase of human biological pathways and processes. *Nucleic Acids Res* **37:** D619-622.

Mukherji, M., R. Bell, L. Supekova, Y. Wang, A.P. Orth, S. Batalov, L. Miraglia, D. Huesken, J. Lange, C. Martin, S. Sahasrabudhe, M. Reinhardt, F. Natt, J. Hall, C. Mickanin, M. Labow, S.K. Chanda, C.Y. Cho, and P.G. Schultz. 2006. Genome-wide functional analysis of human cell-cycle regulators. *Proc Natl Acad Sci U S A* **103:** 14819-14824.

Murray, A.W. 2004. Recycling the cell cycle: cyclins revisited. *Cell* **116:** 221-234.

Newman, M.E.J. 2005. A measure of betweenness centrality based on random walks. *Social Networks* **27:** 39-54.

Downloaded from genome.cshlp.org on October 3, 2011 - Published by Cold Spring Harbor Laboratory Press

Obaya, A.J., M.K. Mateyak, and J.M. Sedivy. 1999. Mysterious liaisons: the relationship between c-Myc and the cell cycle. *Oncogene* **18:** 2934-2941.

Olsen, J.V., M. Vermeulen, A. Santamaria, C. Kumar, M.L. Miller, L.J. Jensen, F. Gnad, J. Cox, T.S. Jensen, E.A. Nigg, S. Brunak, and M. Mann. 2010. Quantitative phosphoproteomics reveals widespread full phosphorylation site occupancy during mitosis. *Sci Signal* **3:** ra3.

Papin, J.A., T. Hunter, B.O. Palsson, and S. Subramaniam. 2005. Reconstruction of cellular signalling networks and analysis of their properties. *Nat Rev Mol Cell Biol* **6:** 99-111.

Plattner, R., L. Kadlec, K.A. DeMali, A. Kazlauskas, and A.M. Pendergast. 1999. c-Abl is activated by growth factors and Src family kinases and has a role in the cellular response to PDGF. *Genes Dev* **13:** 2400-2411.

Santoni-Rugiu, E., J. Falck, N. Mailand, J. Bartek, and J. Lukas. 2000. Involvement of Myc activity in a G(1)/S-promoting mechanism parallel to the pRb/E2F pathway. *Mol Cell Biol* **20:** 3497-3509.

Schaefer, C.F., K. Anthony, S. Krupa, J. Buchoff, M. Day, T. Hannay, and K.H. Buetow. 2009. PID: the Pathway Interaction Database. *Nucleic Acids Res* **37:** D674-679.

Sears, R.C. and J.R. Nevins. 2002. Signaling networks that link cell proliferation and cell fate. *J Biol Chem* **277:** 11617-11620.

Sirvent, A., C. Benistant, and S. Roche. 2008. Cytoplasmic signalling by the c-Abl tyrosine kinase in normal and cancer cells. *Biol Cell* **100:** 617-631.

Tononi, G., O. Sporns, and G.M. Edelman. 1999. Measures of degeneracy and redundancy in biological networks. *Proc Natl Acad Sci U S A* **96:** 3257-3262.

Tu, Z., C. Argmann, K.K. Wong, L.J. Mitnaul, S. Edwards, I.C. Sach, J. Zhu, and E.E. Schadt. 2009. Integrating siRNA and protein-protein interaction data to identify an expanded insulin signaling network. *Genome Res* **19:** 1057-1067.

Vermeulen, K., D.R. Van Bockstaele, and Z.N. Berneman. 2003. The cell cycle: a review of regulation, deregulation and therapeutic targets in cancer. *Cell Prolif* **36:** 131-149.

Vogelstein, B. and K.W. Kinzler. 2004. Cancer genes and the pathways they control. *Nat Med* **10:** 789-799.

Welch, P.J. and J.Y. Wang. 1993. A C-terminal protein-binding domain in the retinoblastoma protein regulates nuclear c-Abl tyrosine kinase in the cell cycle. *Cell* **75:** 779-790.

Welch, P.J. and J.Y. Wang. 1995. Abrogation of retinoblastoma protein function by c-Abl through tyrosine kinase-dependent and -independent mechanisms. *Mol Cell Biol* **15:** 5542-5551.

Zetterberg, A., O. Larsson, and K.G. Wiman. 1995. What is the restriction point? *Curr Opin Cell Biol* **7:** 835-842.

Zhu, X., M. Gerstein, and M. Snyder. 2007. Getting connected: analysis and principles of biological networks. *Genes Dev* **21:** 1010-1024.

Downloaded from genome.cshlp.org on October 3, 2011 - Published by Cold Spring Harbor Laboratory Press

FIGURE LEGENDS.

Figure 1. Design of the siRNA screen and the cell cycle phase-specific effects of the identified targets.

Panel A provides a schematic of the strategy employed to identify genes involved in cell cycle regulation. The overall z-factor obtained for our screen was 0.56, confirming its high overall quality. Details of the design, assay validation, and target verification are provided in the text, Supplementary Experimental Procedures and Supplementary Figures S1 and S2.

Panel B shows the hierarchical clustering of the siRNA hits according to the observed phenotype on cell cycle. The dendogram represents the various clusters of genes identified by our screen for the observed cell cycle distribution pattern. This pattern is based on the normalized z-scores of each of the siRNA hits in the respective cell cycle phases.

Panel C shows the range of observed changes in proliferation rate. The population growth curves of CH1 cells obtained in response to transfection with either non-silencing siRNA (Normal), or with siRNA against each of the validated hits are plotted. Here, cells were plated at 48 h after siRNA transfection (Day 0), and results are plotted in terms of the fold increase in cell number at the indicated time points. Values are the mean of three separate determinations. The subset highlighted by the bracket indicates those target-specific siRNAs that produced a significant increase in the population doubling times (p-value < 0.05, as indicated by the asterisk)

Panel D provides a further analysis wherein the results in panels B and C were combined to determine the effects of siRNA-mediated target silencing on residence time (RT) of the individual cell cycle phases. Changes (Δ), relative to the corresponding values in GFP-silenced cells, in PDT and RT of the individual phases are shown here as

Downloaded from genome.cshlp.org on October 3, 2011 - Published by Cold Spring Harbor Laboratory Press

the mean (± SD, grey bar) of three experiments. Details of their calculation are provided in Supplementary Figure S3.

Figure 2. A systems approach to the analysis of cell cycle regulation and the identification of phase-specific IMP nodes.

Panel A illustrates the rationale underlying the examination of source to target sub-networks in order to identify key intermediate effectors of cell cycle perturbation. Here the sources denote the hits identified by the siRNA, while the targets denote the key molecules involved directly in progression of cell cycle and growth.

Panel B provides the 'source' characterization of the hits obtained in the siRNA screen, based on the phase-specific effects obtained. The genes described here are the human orthologs of the murine counterparts (see Text).

The flow chart in panel C provides a step-wise summary of the *in silico* methodologies employed for eventual identification of the phase-specific regulatory modules. STEP 1 describes the stages involved in delineation of the core network, whereas STEP 2 illustrates the subsequent analysis of this core network to extract the phase-specific IMP node subnetworks. Finally, STEP 3 depicts the stages through which an analysis of the IMP node sub-networks eventually yielded the phase-specific modules. These individual steps are described in detail in Supplementary Experimental Procedures.

Panel D lists the IMP nodes eventually identified through this network analysis for regulation of the G1, S, and G1S phases.

Figure 3. Extraction of phase-specific sub-network and their constituent regulatory motifs.

Downloaded from genome.cshlp.org on October 3, 2011 - Published by Cold Spring Harbor Laboratory Press

Panels A, B, and C describe the phase specific IMP node sub networks extracted from our cell cycle core network for G1, S and G1S phase regulation. The IMP nodes are defined in red, while the blue nodes denote the intermediate node linking any two or more IMP nodes. Panel D provides a compilation of the different functional motifs identified in each of the phases, along with a brief description of their biological implications. In addition, a typical topological representation of each kind of motif is also shown. Here both 3- and 4-node motifs in the FFL categories have been grouped together for the sake of convenience. Panel E compares the number of the different motifs obtained for the integrated IMP node network (Real) versus that in a hundred randomized networks (Random, values given as mean ± S.D.). In these randomizations both the nodes and the number of links were kept at a constant. The statistical significance of the difference in numbers between the Real and Random cases is indicated by the corresponding Z-scores which were calculated as (<Real> - <Random>)/S.D.). Here NS indicates that there was no significant change in the case of scaffolds. This is not surprising given that scaffolds are composed of undirected edges.

Figure 4. Delineating phase-specific regulatory modules and defining the vulnerable nodes.

Panel A summarizes the results of our analysis of centrality measures of the nodes in each of the phase-specific regulatory modules. This is depicted as a Stress versus Betweenness plot for all the molecules in the G1 and G1S cell cycle modules. Only those nodes that are above the cutoff of 2.5 times that of the mean value (indicated by the dotted line, see text) are identified here.

Panels B, C, and D show the IMP node based regulatory modules obtained for each of the individual phases. These represent phase-specific modules extracted by merging the

Downloaded from genome.cshlp.org on October 3, 2011 - Published by Cold Spring Harbor Laboratory Press

motifs identified for the G1, G1S and S phases respectively. The nodes are colour coded according to their betweenness centrality measure. The size of the nodes represents the stress parameter, where the size of the nodes increases with increasing stress value. The gradation of the betweennes values is defined by the color bar.

Panel E depicts the stage-dependent modulation in biochemical activities of the core cell cycle regulatory network spanning from early G1, to completion of the S phase. This is presented as a heat map that defines the percent contribution of signaling, transcription regulatory, DNA replicative, and cell cycle regulatory molecules, in each of the indicated windows.

Figure 5. Vulnerable nodes provide targets for synergistic disruption of the cell cycle.

Panel A shows the effects of inhibition of either AKT or ABL on RTs of the individual phases. The increase in RT (ΔRT) of a given phase, relative to untreated cells, is expressed as a ratio of the corresponding increase- again relative to untreated cells - in PDT (ΔPDT). Here, LY294002 and Imatinib mesylate were used at concentrations that were half of their respective IC_{50} values and the increase in PDT obtained over that of untreated cells was 3h. The effects of perturbation of the remaining high-stress high-betweenness nodes identified in Figure 5A are similarly shown in Panel B. With the exception of SRC, where PP1a was used for inhibition, perturbation was achieved through siRNA-mediated depletion in all cases. Accordingly, the control cells used for the purposes of comparison were those treated with non-silencing (i.e. GFP-specific) siRNA. The results for GRB2 and EP300-silencing are not included as high levels (>80%) of cell death were obtained in these cases. Values in both panels are the mean

Downloaded from genome.cshlp.org on October 3, 2011 - Published by Cold Spring Harbor Laboratory Press

(±SD) of three independent experiments. No significant effect on RT of the G2 phase was noted in any of the cases. See also Supplementary Figure S4.

Panel C depicts the dose-response profile for apoptosis in CH1 cells treated with pharmacological inhibitors of the indicated kinases. Doses for each inhibitor used were in multiples of their corresponding IC_{50} values as noted. Values (mean ± S.D. of three experiments) are expressed as the percent of apoptotic cells obtained 72h later, after normalizing for spontaneous apoptosis. The bar graph in Panel D shows the corresponding accumulation of CH1 cells in the G1 phase obtained at 18h with the 5 x IC_{50} concentration of inhibitors. Values (mean ± S.D. of three experiments) are expressed as the increase in percent of the G1 population, over that in untreated cells.

Panel E lists the target kinases examined, their phase-specificity, the pharmacological inhibitors employed for inhibition of these kinases, and the corresponding IC_{50} values of these inhibitors.

In Panel F, CH1 cells were treated with inhibitors against the indicated kinases (or kinase combinations) and the consequent effect on cellular apoptosis was determined at 48h later. The concentration of the relevant inhibitor employed was five-fold greater than its corresponding IC_{50} value in all cases and results are the mean (± S.D.) of three experiments. For the panels D, E and F, cells were treated with a single addition of the inhibitor, or, inhibitor combination.

Figure 6. Network of core pathways that mediate commitment of cells to the division cycle.

In the pathway model the nodes in red are proteins which are present in the G1 and/or G1S modules. Nodes present in green are derived from literature (they include intermediates or effectors of cellular processes captured by our merged modules). The grey arrows depict interactions taken from the merged G1 and G1S modules. The blue

Downloaded from genome.cshlp.org on October 3, 2011 - Published by Cold Spring Harbor Laboratory Press

arrows are links added from literature. The dotted orange boxes highlight cellular signaling pathways and the dotted grey boxes group molecules involved in regulating similar cellular processes. The dashed blue arrows indicate a known role of the source node in regulating the target node, derived from literature.AKT and PTK2B are G1 specific high-stress and betweeness nodes. SRC and GRB2 show high stress and betweeness in both modules. ABL and JUN are present as high stress- betweeness nodes only in the G1S modules. A detailed description of the pathways captured is given in the supplementary information.

Figure 7. Vulnerable nodes constitute regulatory elements that are conserved across a broad range of cell types.

The effects of combined inhibition of the indicated kinase combinations (at concentrations of 5 x IC_{50} values) on fourteen different cancer cell lines, following a protocol similar to that described for Figure 6F, are shown in Panel A, whereas Panel B shows the results of a similar experiment with indicated inhibitor combinations performed on normal B-lymphocytes purified from the peripheral blood of six different individuals. Panel C gives the CI values for the combined inhibition of AKT and ABL obtained for the individual cell lines. CI values were calculated as previously described (Chou and Talalay 1981). For four cell lines CI values could not be estimated since either one (for Namalwa and THP1) or both (for Jurkat and A549) inhibitors showed no effect when added individually (indicated as broken bars). The red line defines the cut-off (CI=1) for interpreting responses as being synergistic and values are the mean (± S.D.) of three determinations. Panel D shows representative results for the synergy between AKT and ABL inhibition where one (Namalwa) or both (Jurkat) inhibitors were ineffective when added individually.

Downloaded from genome.cshlp.org on October 3, 2011 - Published by Cold Spring Harbor Laboratory Press

Panel E shows the effects of the inclusion of PP1a, in addition to LY294002 and Imatinib mesylate, on the apoptotic responses of HEK293 and HEPG2 cells. Results are shown in two sub-panels for each cell line where the sub-panel on the left indicates the effects either of LY294002, Imatinib mesylate alone (each at 4 x IC_{50}), or a combination of both. The sub-panel on the right gives the results of addition of increasing concentrations of PP1a either alone (blue line), or in the presence of the combined inhibitors for AKT and ABL (each at 4 x IC_{50}, red line). Values again are the mean (± S.D.) of three determinations.

.

Downloaded from genome.cshlp.org on October 3, 2011 - Published by Cold Spring Harbor Laboratory Press

Figure 1

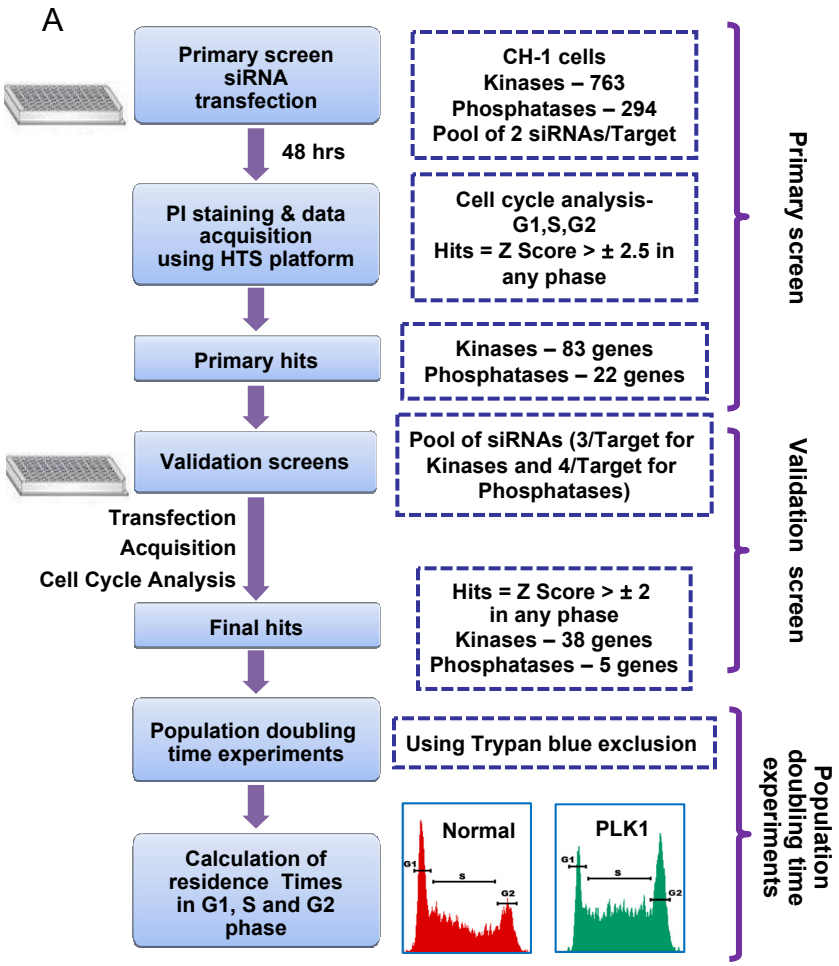

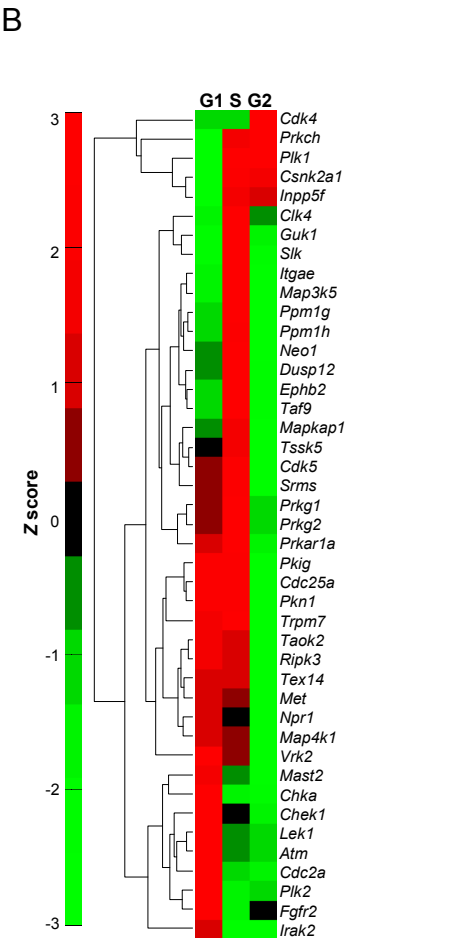

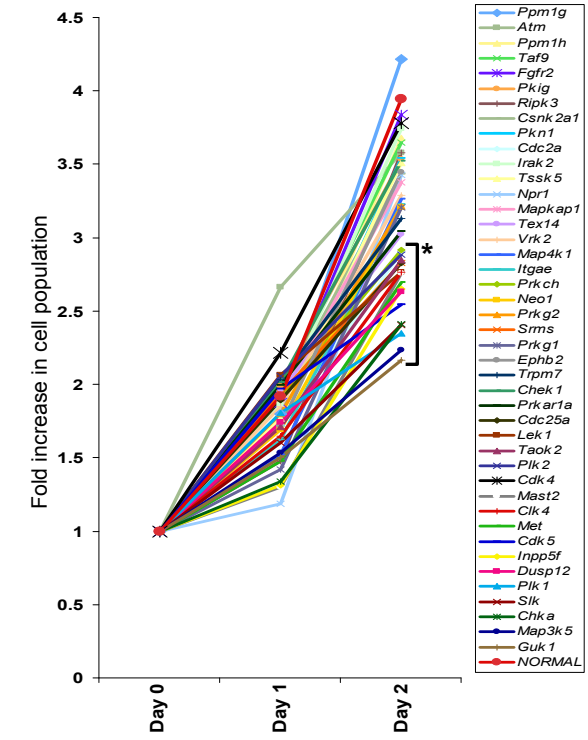

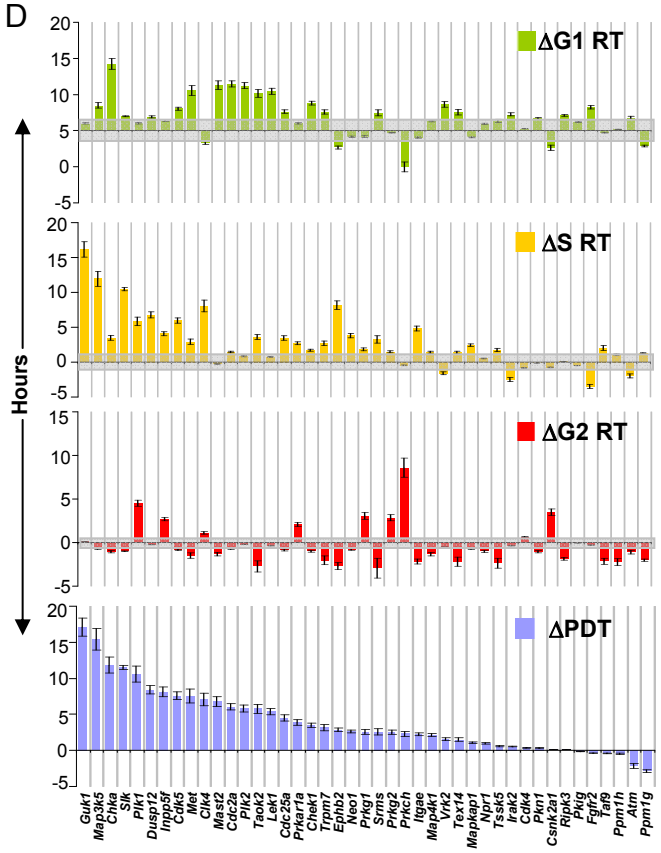

Figure 2

A

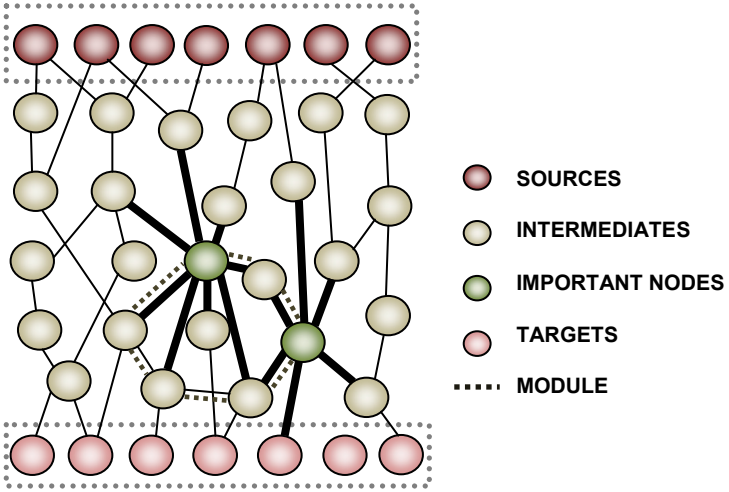

B

List of Cell Cycle Phase Specific Sources		
G1 Sources	**S Sources**	**G1S Sources**
PKIG	ITGAE	TRPM7
VRK2	EPHB2	NPR1
CHEK1	MAPKAP1	PRKAR1A
FGFR2	NEO1	SRMS
MAST2	PPM1H	TSSK5
RIPK3	PPM1G	MET
ATM	TAF9	CDC2A
IRAK2	GUK1	CDC25A
PLK2	CLK4	TAOK2
LEK1		SLK
PKN1		CDK5
TEX14		MAP3K5
		DUSP12
		MAP4K1

C

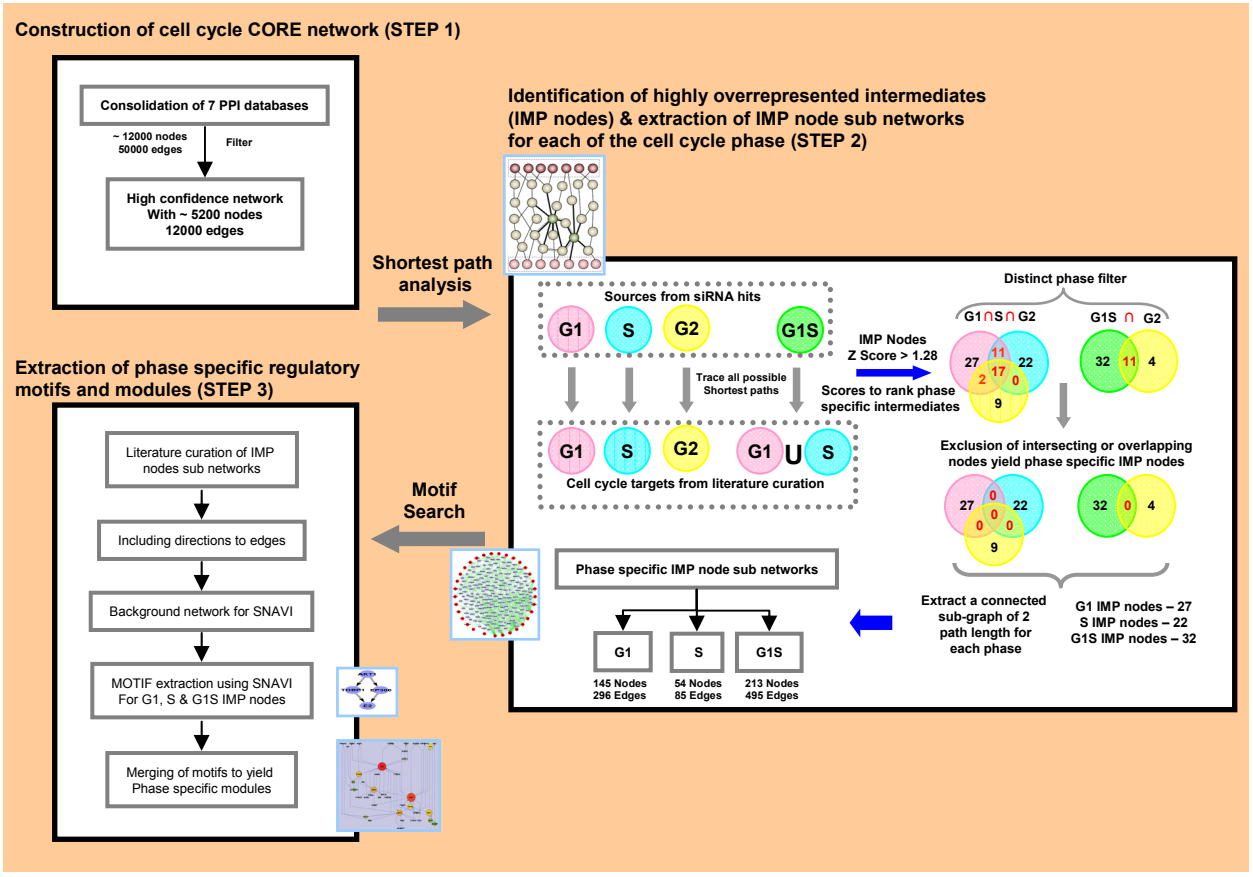

D

List of Cell Cycle Phase Specific IMP Nodes					
G1 Phase		**S Phase**		**G1S Phase**	
PTK2B	CSNK2A1	ITGB7	RBL1	ABL1	LYN
TICAM2	WT1	ADORA2B	CCNA2	ANXA1	GADD45G
KIF23	NFKBIA	NTN1	DAB1	GRB2	SKP2
YWHAQ	TICAM1	FOS	ETF1	RIS2	CDKN1B
BCL2	DLGAP4	YWHAG	COIL	SRC	CSNK2A1
IKBKAP	E2F1	PIN1	GRIN2B	RB1	CDC25A
MAPK8	MYC	CSE1L		UBB	ELK1
ESR1	LCK	DOK1		AKT1	JUN
PTEN	TANK	DCC		EP300	TOPBP1
AKT1	XRCC6	RIS2		BRCA1	E2F1
SRC	TRIM27	STAT1		MCM7	MYC
ARHGEF7		E7		ESR1	TUBA4A
ZBTB17		EZR		POLR2A	EPC1
EEF1D		PKM2		STAT1	WT1
GRB2		EED		MAPK3	PTPN2
SYNGAP1		TAF1		CCNA2	CCND1

Downloaded from genome.cshlp.org on October 3, 2011 - Published by Cold Spring Harbor Laboratory Press

Downloaded from genome.cshlp.org on October 3, 2011 - Published by Cold Spring Harbor Laboratory Press

Figure 3

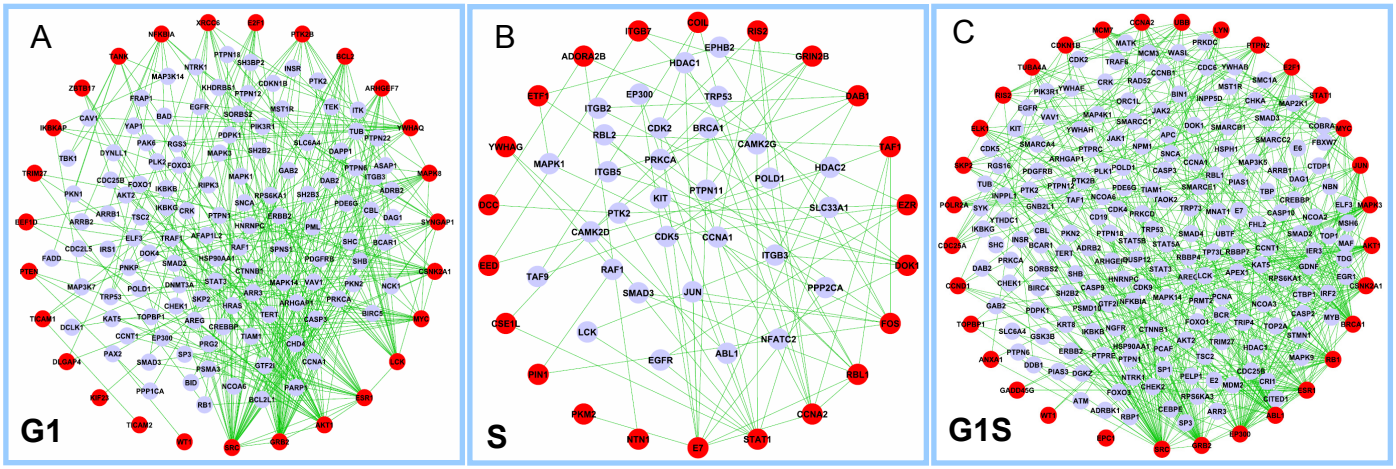

D

Motif	Structure	Biological significance	Occurrences in phase specific network			Example
			G1	S	G1S	
Scaffold	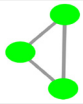	Signal localization and amplification	13	6	28	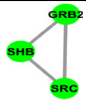
Feed forward loop	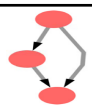	Noise filter and signal dynamics	10	1	43	
Bifan	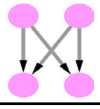	Signal synchronization	2	0	16	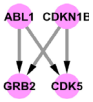
Diamond	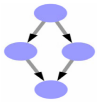	Reflection of redundancy in the system	3	0	18	

E

Motif	Occurrences of Motifs		Z Score
	Real	Random	
Scaffold	37	37±7	NS
Feed forward loop	44	12±4	8
Bifan	16	5±2	5.5
Diamond	20	4±2	8

Downloaded from genome.cshlp.org on October 3, 2011 - Published by Cold Spring Harbor Laboratory Press

Figure 4

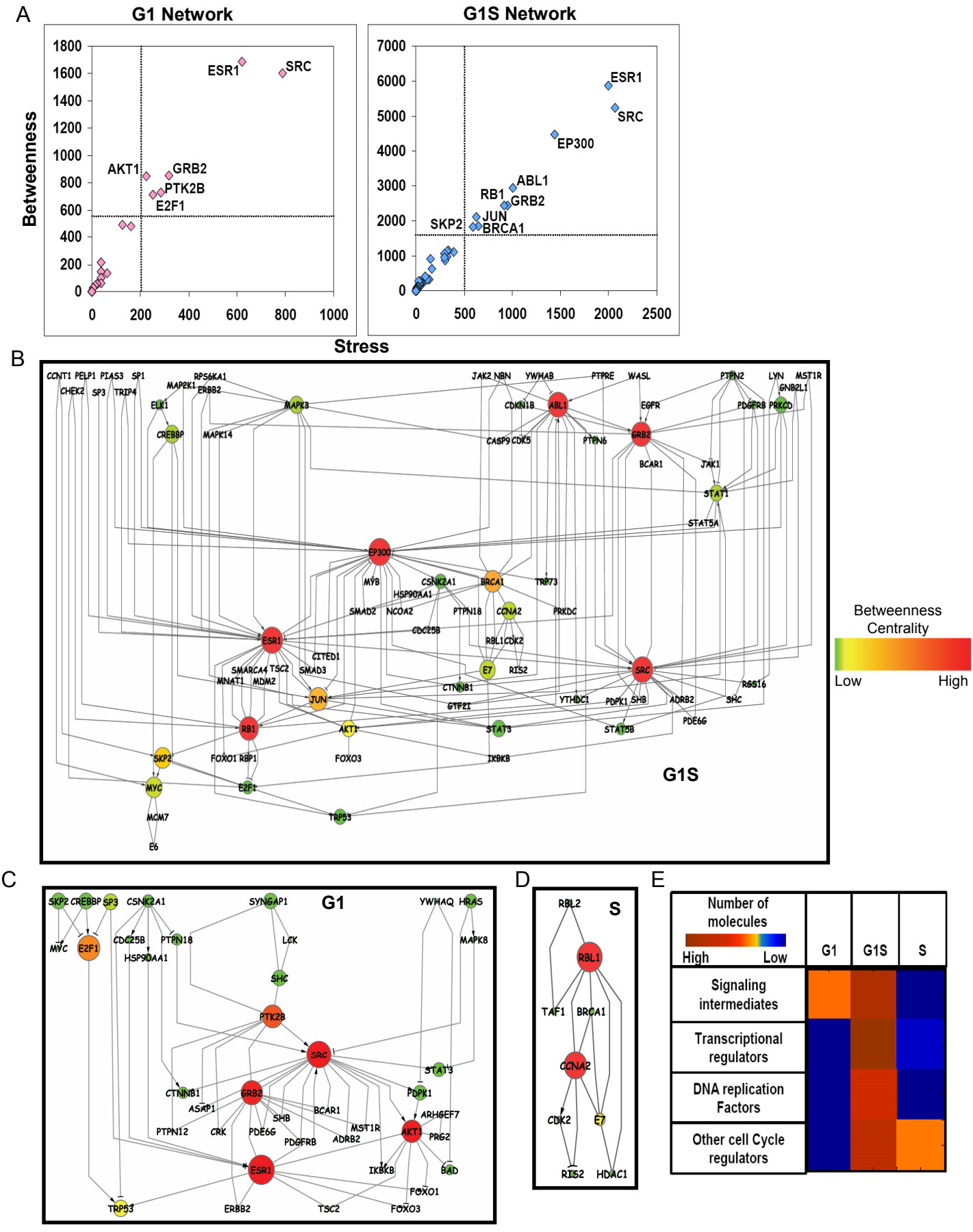

Downloaded from genome.cshlp.org on October 3, 2011 - Published by Cold Spring Harbor Laboratory Press

Figure 5

A

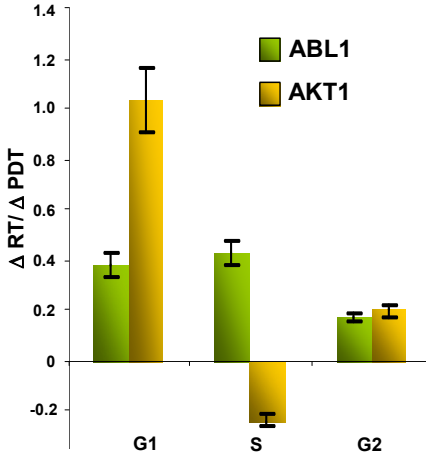

B

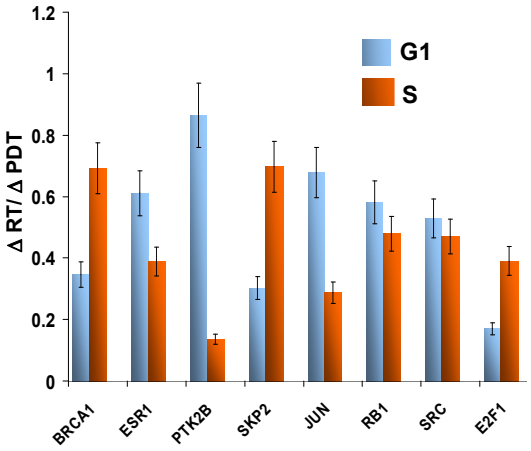

C

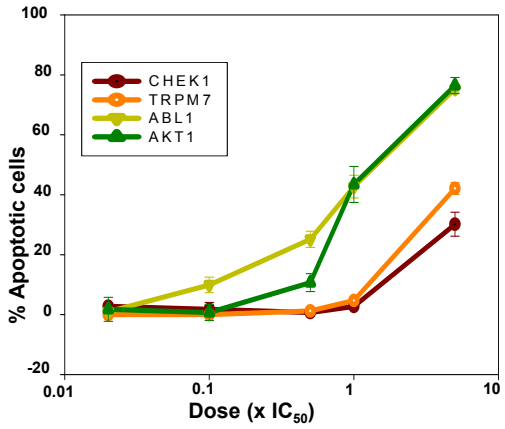

D

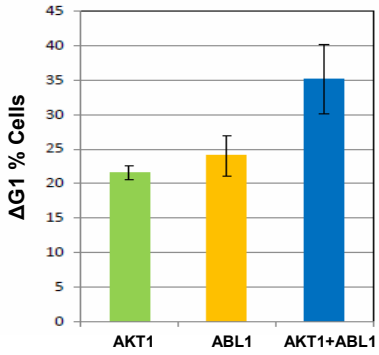

E

TARGET KINASE	PHASE SPECIFICITY	INHIBITOR USED	IC_{50}
ABL1	G1 and S	Imatinib Mesylate	0.25 μM
AKT1	G1	LY294002	6.6 μM
CHEK1	G1	TCS 2312	60 nM
TRPM7	G1 and S	2-APB	10 μM
FGFR2	G1	PD 173074	3.3 nM
PKA (PRKAR1A)	G1 and S	KT 5720	60 nM
MET	G1 and S	PHA-665752	9 nM
SRC	G1 and S	PP1a	200 nM

F

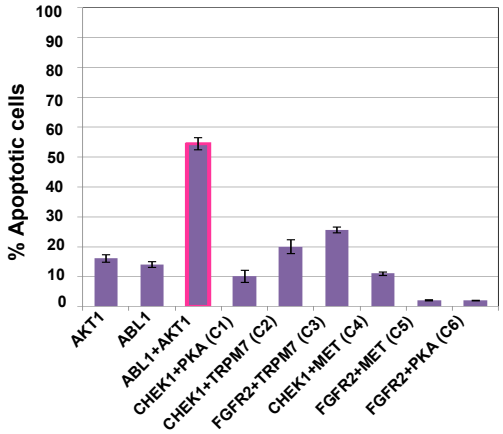

Downloaded from genome.cshlp.org on October 3, 2011 - Published by Cold Spring Harbor Laboratory Press

Figure 6

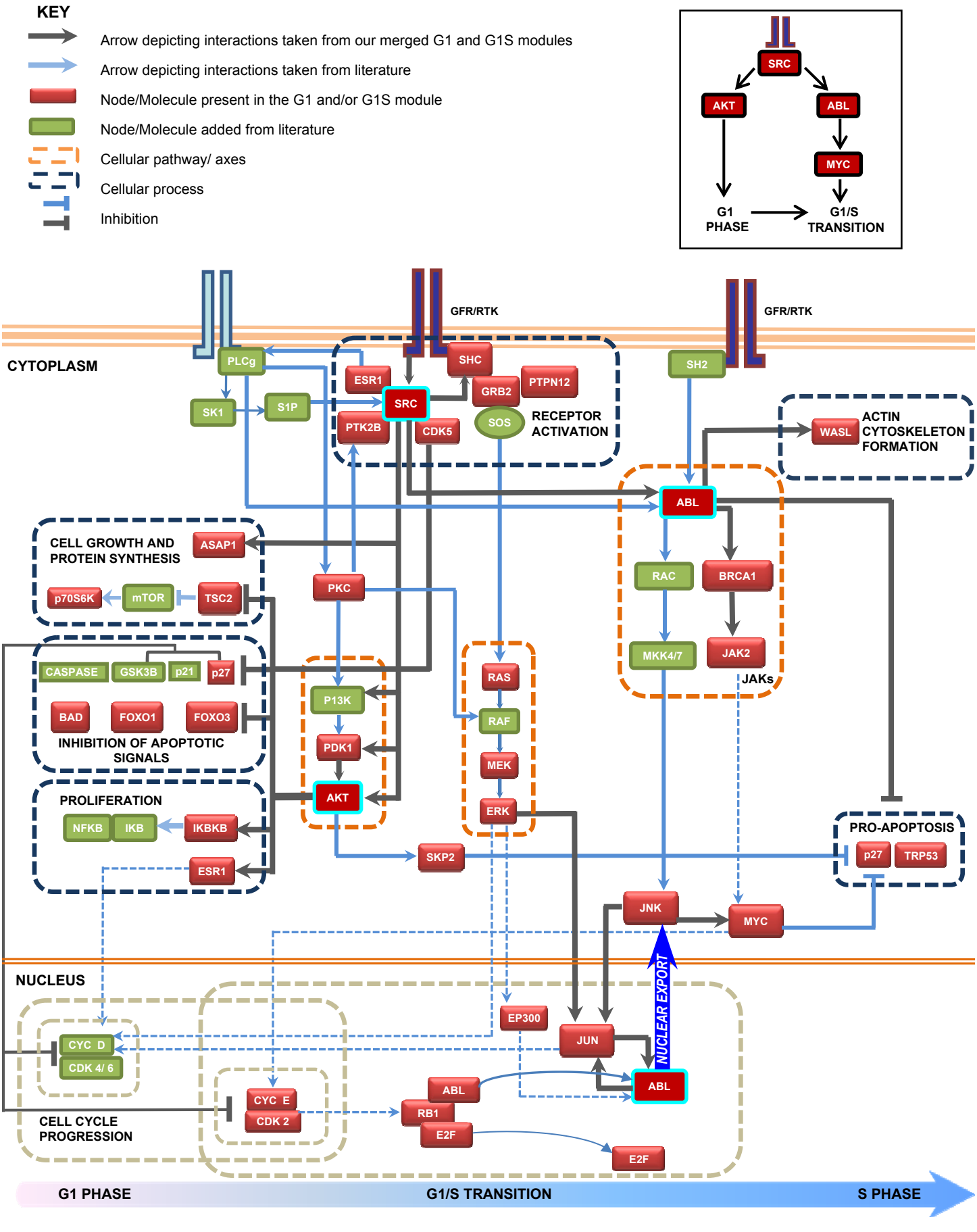

Downloaded from genome.cshlp.org on October 3, 2011 - Published by Cold Spring Harbor Laboratory Press
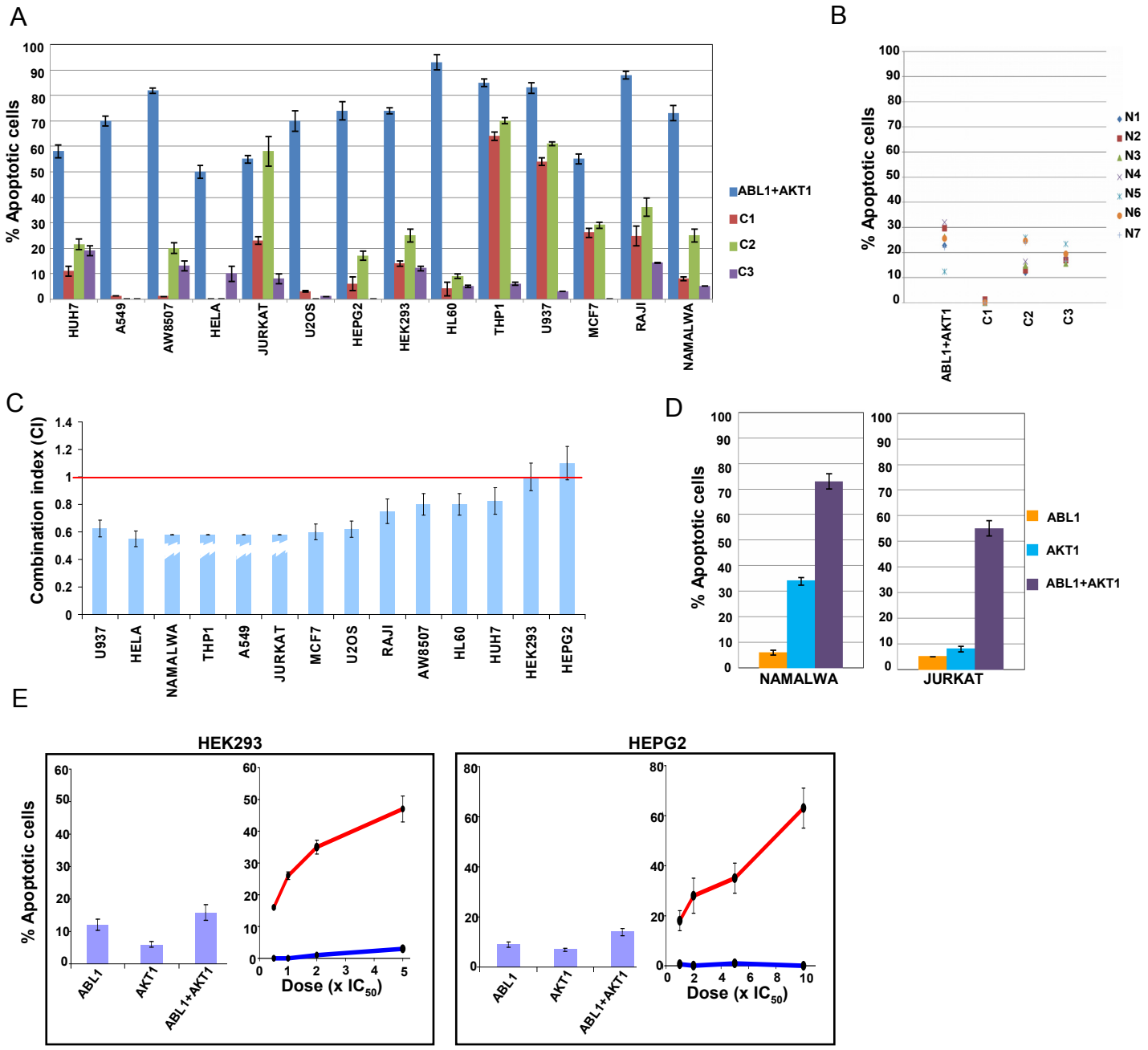
Figure 7